NeuroImage 135 (2016) 253–260

Contents lists available at ScienceDirect

NeuroImage

journal homepage: www.elsevier.com/locate/ynimg

Improving the specificity of R_2' to the deoxyhaemoglobin content of brain tissue: Prospective correction of macroscopic magnetic field gradients

Nicholas P. Blockley *, Alan J. Stone

FMRIB Centre, Nuffield Department of Clinical Neurosciences, University of Oxford, Oxford, UK

ARTICLE INFO

Article history:
Received 2 December 2015
Revised 30 March 2016
Accepted 6 April 2016
Available online 3 May 2016

Keywords:
R_2' contrast
Relaxometry
Image artifact reduction
Deoxyhaemoglobin
Oxygen metabolism

ABSTRACT

The reversible transverse relaxation rate, R_2', is sensitive to the deoxyhaemoglobin content of brain tissue, enabling information about the oxygen extraction fraction to be obtained. However, R_2' is also sensitive to macroscopic magnetic field gradients, particularly at air-tissue interfaces where a large susceptibility difference is present. It is important that this latter effect is minimised in order to produce meaningful estimates of blood oxygenation. Therefore, the aim of this study was to implement a technique to prospectively correct for the effect of susceptibility induced magnetic field gradients on R_2' weighted data. This was achieved by combining the Gradient-Echo Slice Excitation Profile Imaging (GESEPI) technique with an Asymmetric Spin Echo (ASE) pulse sequence. The main advantages of this approach are (i) shorter acquisition times, since a separately acquired magnetic field map is not required and (ii) simpler analysis, since retrospective correction for the effects of magnetic field gradients in postprocessing is not required. In these experiments we show that with this newly developed technique it is possible to correct the majority of grey matter voxels for the expected distribution of through-slice magnetic field gradients to produce maps of R_2' in a short scan duration.

Introduction

Measurements of the reversible transverse relaxation rate, R_2', are commonly used to extract information about the deoxyhaemoglobin content of brain tissue (Fujita et al., 2003). This information has been used to calibrate the BOLD response (Blockley et al., 2012, 2015) or, when combined with information about the deoxygenated blood volume (DBV), measure the resting oxygen extraction fraction (OEF) (An and Lin, 2000; He and Yablonskiy, 2007). This is possible because R_2' is sensitive to the magnetic field inhomogeneity that results from the susceptibility difference between deoxygenated blood in the vessels and the tissue that surrounds them. The same principle has also been used to assess brain iron concentration using measurements of R_2' (Ordidge et al., 1994; Sedlacik et al., 2013). However, R_2' is also sensitive to macroscopic magnetic field inhomogeneity on the scale of the head, particularly due to susceptibility differences at air–tissue interfaces such as the nasal sinuses and ear canals. Left uncorrected the specificity of measurements of R_2' to deoxyhaemoglobin is reduced and derived physiological estimates may become a function of the homogeneity of the magnetic field.

R_2' is most commonly measured using the Gradient Echo Sampling of Spin Echo (GESSE) (Yablonskiy, 1998), Gradient Echo Sampling of FID and Echo (GESFIDE) (Ma and Wehrli, 1996) or Asymmetric Spin Echo (ASE) (Wismer et al., 1988) pulse sequences. The image contrast in GESSE and GESFIDE is not only weighted by R_2', but also by R_2 — the irreversible transverse relaxation rate. These effects can be separated using characteristics of the R_2' weighted signal decay, such as symmetry with respect to the spin echo (An and Lin, 2000) or quadratic exponential decay of the signal around the spin echo (He and Yablonskiy, 2007). In contrast the ASE method allows the R_2' weighting of images to be manipulated with constant R_2 weighting (An and Lin, 2003). This enables R_2' to be fitted directly without assumptions of symmetry or needing to acquire images close to the spin echo. However, to measure the OEF the latter data may still be required to estimate DBV (An and Lin, 2000; He and Yablonskiy, 2007).

All of these methods are sensitive to the effects of susceptibility induced magnetic field gradients (MFGs) due to macroscopic field inhomogeneity i.e. enhanced signal attenuation leading to elevated estimates of R_2'. Typically this effect is corrected retrospectively using a magnetic field map (Yablonskiy, 1998). However, the accuracy of this approach is dependent on the quality of the magnetic field map, often necessitating the separate acquisition of a high resolution field map (He and Yablonskiy, 2007). Alternatively, there are two approaches for reducing signal loss due to through-slice MFGs during data acquisition; either reducing the slice thickness or through the application of a compensatory gradient. The former approach exploits the fact that the signal attenuation due to a through-slice MFG is non-linearly dependent on slice thickness (Yablonskiy, 1998). Therefore, averaging multiple thin slices with equivalent coverage to a single thick slice will reduce signal

* Corresponding author at: FMRIB Centre, Nuffield Department of Clinical Neurosciences, University of Oxford, John Radcliffe Hospital, Headington, Oxford, OX3 9DU, UK.
E-mail address: nicholas.blockley@ndcn.ox.ac.uk (N.P. Blockley).

http://dx.doi.org/10.1016/j.neuroimage.2016.04.013

attenuation. We previously used this technique, known as SubSlice AVEraging (SSAVE) (Wadghiri et al., 2001), to demonstrate the potential of R_2' calibrated BOLD (Blockley et al., 2015). Alternatively compensatory gradients may be used, as previously demonstrated in an R_2' mapping study of iron deposition in the brain (Ordidge et al., 1994). This technique, most commonly known as z-shimming, works by collecting a series of images with different modifications to the amplitude of the rephasing gradient that follows slice selection (Frahm et al., 1988). The modified rephasing gradient amplitude enables local magnetic field gradients to be compensated, but will also produce signal attenuation in regions of the brain where MFGs are minimal. Therefore the resultant dataset must be combined in such a way as to preserve the optimal signal at each voxel location (Constable, 1995; Ordidge et al., 1994). Alternatively the modification of the rephasing gradient can be considered as phase encoding in the third dimension. In this interpretation z-shimming is equivalent to high resolution 3D imaging whereby a Fourier transform is used to integrate over the z-shim levels. This idea was exploited in the Gradient Echo Slice Excitation Profile Imaging (GESEPI) technique, which is essentially a 3D sequence oversampled in the slice direction (Yang et al., 1998). Encoding multiple thin slices in this way reduces the signal to noise ratio (SNR) of the resultant images and therefore several slices are typically averaged together to improve SNR.

The aim of this study was to implement a technique to combine prospective correction of susceptibility induced MFGs with direct acquisition of R_2' weighted images. This was achieved by combining the GESEPI technique with an ASE pulse sequence, which we term GESEPI ASE (GASE) (see Fig. 1). The main advantages of this approach are (i) shorter acquisition times, since a separately acquired magnetic field map is not required and (ii) simpler analysis, since retrospective correction for the effects of magnetic field gradients in postprocessing is not required. In these experiments we show that the GASE pulse sequence is able to reduce the effect of susceptibility induced MFGs on maps of R_2' in a short scan duration.

Methods

The implementation of GASE was performed in three steps. Firstly, the sequence was tested in a standard phantom with MFGs imposed by perturbing the linear shim gradients of the scanner. Secondly, the maximum MFG that can be compensated by GESEPI is determined by the maximum phase encoding gradient moment in the z-direction and the spin echo displacement time, τ. In practice, a range of τ values are employed to modulate the R_2' weighting of images in an ASE experiment. Therefore, the sequence must be optimised for the worst case scenario i.e. the maximum MFG in the region of interest and the maximum τ value. The maximum τ in these experiments was 30 ms, but the maximum z-gradient was unknown. To examine the magnitude of these MFGs high resolution magnetic field mapping was performed in a small cohort of subjects. Finally, informed by this analysis several GASE variants were tested on a separate cohort of subjects and compared with the standard ASE sequence.

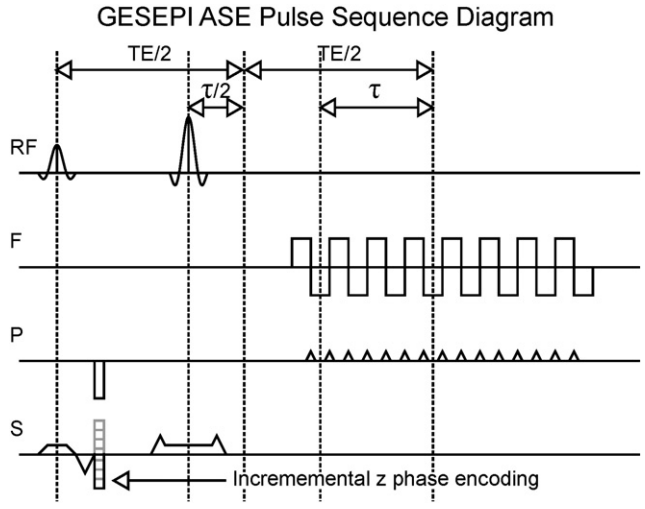

Fig. 1. Pulse sequence diagram of the GESEPI ASE (GASE) technique. ASE: The 180° refocussing pulse is shifted by a time $\tau/2$ resulting in the formation of a spin echo at time τ before the centre of the readout. A range of τ values are acquired to introduce different degrees of R_2' weighting. However, since TE is constant the degree of R_2 weighting is constant. GESEPI: In-plane phase encoding is supplemented by phase encoding in the z (slice) direction. The maximum z phase encoding value determines the maximum through slice magnetic field gradient (MFG) that can be compensated.

Imaging

All imaging was performed on a Siemens Verio 3T scanner (Siemens Healthcare, Erlangen, Germany) using the body transmit coil and a 32 channel receive coil. Healthy volunteer subjects were scanned under a technical development protocol agreed with local ethics and institutional committees. Slices were acquired parallel to the AC–PC line and therefore locations in the following text are described with reference to the slice position, i.e. superior–inferior (SI) is used synonymously with the z-axis (through-slice), anterior–posterior (AP) with the y-axis and left–right (LR) with the x-axis.

For the field mapping experiments, high resolution images were acquired using a 2D FLASH method with FOV 240 mm, 192 × 192 matrix, slice thickness 2 mm, slice gap 0.5 mm and 75 slices. The repetition time (TR) was set to 1000 ms and two echoes were acquired with echo times (TE) of 5.19 ms and 7.65 ms giving a TE difference of 2.46 ms. Two signal averages were acquired.

ASE and GASE data were acquired with a common set of parameters; a field of view (FOV) of 240 mm, slice/slab thickness 5 mm, slice/slab gap 2.5 mm, 20 slices/slabs, TR 3000 ms and TE 44 ms. Slices/slabs were acquired in an interleaved order and phase encoded in the AP direction. Raw data were Hanning filtered prior to reconstruction. Six different R_2' weightings were acquired with τ values of 15, 18, 21, 24, 27 and 30 ms. To be clear, in the standard ASE sequence multiple 5 mm thick 2D slices were acquired, whereas in the GASE variants multiple 5 mm thick 3D encoded slabs were acquired. The degree of this z-encoding is described below for each variant.

In addition, T_1 weighted structural scans were acquired for co-registration and segmentation purposes using a 3D Magnetisation Prepared Rapid Acquisition Gradient Echo (MPRAGE) sequence (Mugler and Brookeman, 1990). The following sequence parameters were used; 192 × 192 × 174 matrix, resolution 1 × 1 × 1 mm^3, TR 2040 ms, TE 4.7 ms, inversion time (TI) 900 ms and flip angle 8°.

GESEPI MFG compensation

The maximum MFG compensation provided by the GESEPI technique is determined by the maximum phase encoding gradient moment. In the presence of an opposing susceptibility induced MFG this enables the centre of the echo to be captured within the sampling window. The magnitude of this gradient moment is determined by the voxel dimension, Δz. Therefore, a local susceptibility induced MFG, G_{MFG}, will only be compensated for a given τ value when,

$$G_{MFG}(\tau) \leq \frac{\pi}{\gamma \Delta z \tau} \quad (1)$$

where γ is the proton gyromagnetic ratio (267.5×10^6 rad s^{-1} T^{-1}) (Reichenbach et al., 1997). Beyond this critical value of G_{MFG} the centre of the echo will begin to exit the sampling window and the signal will be rapidly attenuated. In contrast, for two dimensional slice selective images, signal attenuation is always present when $G_{MFG} \neq 0$. Under the assumption of a rectangular slice profile and a linear through-slice

gradient the relative signal attenuation, $|F(\tau)|$, can be described by a sinc function (Yablonskiy, 1998).

$$|F(\tau)| = \left|\frac{\sin(\gamma G_{MFG}\Delta z\tau/2)}{\gamma G_{MFG}\Delta z\tau/2}\right| \quad (2)$$

Four variants of the ASE sequence were used, henceforth referred to as ASE, GASE 4, GASE 8 and GASE 128. The ASE variant consisted of a standard 2D EPI acquisition without correction for MFGs in the z-direction. Therefore, following (2), non-zero values of G_{MFG} will lead to signal attenuation. Images at each τ value were averaged over 8 repetitions. The GASE 4 variant included GESEPI correction by phase encoding each 5 mm slice into 4 partitions in the z-direction, each 1.25 mm thick. From (1) the critical value of G_{MFG} in the z-direction at the maximum τ value is $G_{MFG}(\tau = 30\text{ ms}) = 313\ \mu T\ m^{-1}$. GASE 4 was acquired with 100% partition oversampling to prevent aliasing in the z-direction and resulting in the acquisition of 8 partitions per τ value. The scan duration of the ASE and GASE 4 variants was 2 min 24 s. The GASE 8 variant doubled the number of partitions to 8, each with a thickness of 0.63 mm, to give a critical value of $G_{MFG}(\tau = 30\text{ ms}) = 621\ \mu T\ m^{-1}$ in the z-direction. To investigate the potential for compensating in-plane MFGs a further variant was tested, GASE 128. Whilst Eq. (1) was derived for phase encoding in the z direction, this equation holds more generally for in-plane phase encoding (y) and frequency encoding (x) (Reichenbach et al., 1997).

$$\text{In-plane phase encoding}: \quad G_{MFG}(\tau) \le \frac{\pi}{\gamma\Delta y\tau}. \quad (3)$$

$$\text{Frequency encoding}: \quad G_{MFG}(\tau) \le \frac{\pi}{\gamma\Delta x\tau}. \quad (4)$$

Therefore, increasing the in-plane resolution for the same field of view will increase the maximum MFG that can be compensated (i.e. by enabling the shifted centre of k-space to be captured within the sampling window). Since an echoplanar acquisition is used in these experiments this approach may be limited where MFGs are particularly large in one of these dimensions leading to shearing of the k-space trajectory (Weiskopf et al., 2007). GASE 128 was based on GASE 4, but with a segmented 128 × 128 matrix (2 shots, EPI factor 64). This increase in resolution represents a doubling of the in-plane compensation for MFGs; in-plane $G_{MFG}(\tau = 30\text{ ms}) = 104\ \mu T\ m^{-1}$ for 64 × 64 matrix versus in-plane $G_{MFG}(\tau = 30\text{ ms}) = 208\ \mu T\ m^{-1}$ for 128 × 128 matrix. In addition the following parameters were altered: TE 50 ms and bandwidth 1954 Hz/px. Both GASE 8 and GASE 128 retain 100% partition oversampling and since both also require twice as many TR periods, the scan duration of these variants was 4 min 48 s.

Phantom experiments

The effectiveness of the GESEPI correction was first tested using an agar gel phantom based on the design proposed by the Functional Bioinformatics Research Network (FBIRN) consortium (Friedman and Glover, 2006). Due to the homogenous construction of the phantom, aside from the presence of small bubbles, signal decay is dominated by T_2 processes. Therefore, under the assumption that the phantom is well shimmed, shifting the refocusing pulse in the ASE pulse sequence should have only a minimal effect on the measured signal amplitude. The phantom was placed in the centre of the receive coil, which was then placed at the isocentre of the magnet. Shimming was performed using the manufacturer's standard image based shimming procedure. A single axial slice through the centre of the phantom was prescribed and images were acquired using the standard ASE acquisition and the GASE 4 protocol. The shim values were then manually changed to impose a gradient across the imaging slice of approximately $100\ \mu T\ m^{-1}$. The ASE and GASE 4 protocols were then re-run.

The following pre-processing steps were performed. ASE data were averaged over the 8 repeats at each τ value. For GASE 4 the oversampled partitions were discarded and the central 4 partitions averaged at each τ value. Linear regression of the log magnitude signal versus τ was used (Eq. (5)), assuming constant R_2 signal weighting, to estimate constant and R_2' terms.

$$S = S_0 e^{-TER_2} e^{-\tau R'_2} \quad (5)$$

MFG mapping

High resolution field mapping was performed to assess the magnitude of the susceptibility induced MFGs in the average subject. Four healthy volunteers were recruited (age range 23–29 years old, 2 females) and underwent the field mapping protocol detailed above. FSL tools were used to prepare and regularise the fieldmaps using a Gaussian smoothing kernel with $\sigma = 1$ mm (Jenkinson et al., 2012). Further processing was performed in MATLAB (The Mathworks, Natick, MA) to calculate the gradient of the magnetic field maps numerically using a central differences approach (gradient function in MATLAB) in units of $\mu T\ m^{-1}$. Gradients were calculated for each of the three orthogonal axes of the prescribed imaging volume, i.e. z-axis approximately in the foot–head direction, y-axis in the anterior–posterior direction and x-axis in the left–right direction. Slices were placed parallel to the AC–PC line for consistency across subjects. Group maps were created by non-linear registration of the brain extracted (Smith, 2002) magnitude FLASH images to MNI152 space (Mazziotta et al., 2001) via a structural scan (Jenkinson et al., 2002, 2012).

A voxel level analysis of the magnitude and distribution of susceptibility induced MFGs was performed. Regions of interest (ROIs) were generated from the MNI structural atlas (Collins et al., 1995) and transformed into the native space of each subject's field map. These structural ROIs were masked with a grey matter mask created from automatic segmentation of the structural scan using FAST (FMRIB's Automated Segmentation Tool) (Zhang et al., 2001). ROIs were formed for the frontal, insula, occipital, parietal and temporal cortices plus the cerebellum. Furthermore a cortical region of interest was generated by combining all of the regions excluding the cerebellum. Due to the skewed distribution of the measured MFGs the following percentiles were calculated: 0.5%, 2.5%, 25%, 50% (median), 75%, 97.5%, 99.5%.

GASE experiments

ASE and GASE data were acquired in six healthy subjects (age range 23–41, 2 females). All three variants of the GASE sequence were acquired, plus an uncorrected ASE data set. Slices were prescribed to cover the whole brain and the same prescription was used for all four scans.

Similar pre-processing steps to the phantom experiments were followed. ASE data were averaged over the 8 repeats at each τ value and GASE data was averaged over the acquired number of partitions (4 or 8). The in-plane resolution of the GASE 128 data was collapsed to the same matrix size and resolution as the other data sets by averaging adjacent pairs of voxels. Maps of R_2' were created by linear regression of the log magnitude signal versus τ (Eq. (5)).

A voxel level analysis of the measured R_2' values was performed for the same ROIs as defined in the field mapping experiments above. Initial histogram analysis (not shown) revealed long tales to the distribution of R_2' values. The asymmetry in the distribution is attributed to the fact that MFGs are expected to be relatively small in the majority of the brain following shimming. However, a small but significant number of voxels will see much larger MFGs and hence generate much larger R_2' values. Therefore, in order to provide representative group statistics the median and interquartile range of each of the ROIs were calculated to assess regional and sequence variant differences.

Results

The effectiveness of the GESEPI correction was demonstrated in a phantom study (Fig. 2). Images were acquired with the ASE and GASE 4 protocols following the standard shimming procedure (Fig. 2a, c) and with an imposed gradient in the through-slice direction (Fig. 2b, d). For the standard shim both ASE and GASE 4 show similar low levels of signal decay as a function of τ and minimal R_2' values. However, with a gradient imposed a large amount of signal decay is observed in the ASE sequence leading to high R_2' values, whilst the GASE 4 data is largely unaffected and comparable to the standard shim images.

Field mapping reveals a large degree of regional variation with the largest MFGs found in inferior areas of the brain (Fig. 3). The regional variations for all three axes are displayed in Table 1. The brain regions most affected by MFGs in the z-direction are the frontal and temporal lobes, with the insula least affected.

Fig. 4 shows R_2' maps for all four pulse sequence variants. Large values of R_2' are particularly visible in the ASE data in the frontal and temporal regions (Fig. 4a). Table 2 shows the median and interquartile range (IQR) for each of the seven ROIs and four sequence variants. For regions shown to have a greater fraction of large MFGs (frontal and temporal) the increasing levels of compensation provided by the GASE sequence reduces both the median and IQR. In regions that are only mildly affected by MFGs (insula) the median and IQR are largely unchanged by increasing levels of compensation. When comparing GASE variants it can be seen that there is only a minor reduction in median and IQR between GASE 4 and GASE 8. Further reductions can be seen when comparison is made with GASE 128, particularly in the temporal lobe where in-plane gradients were observed to be greatest (Table 1).

A non-parametric one-way analysis of variance test (Kruskal–Wallis) revealed that the distributions of R_2' values as measured by all four sequence variants in the cortex ROI are not all identical ($p < 0.0001$). Furthermore, a multiple comparison test of each of the possible sequence pairs shows that ASE R_2' values have a significantly different distribution than the GASE 4, GASE 8 and GASE 128 sequence variants ($p < 0.0001$). Similarly, GASE 128 is significantly different to GASE 4 and GASE 8 ($p < 0.0001$). However, no significant difference was detected between GASE 4 and GASE 8 ($p = 0.86$).

Fig. 5 highlights the regions of the brain that are most improved by the GASE sequence variants. Comparing ASE with GASE 4 reveals improvements around the nasal sinuses and ear canals (Fig. 5a). Further improvements are made when comparing GASE 4 with GASE 8 (Fig. 5b) or GASE 128 (Fig. 5c), although they are small and largely confined to the inferior portions of the brain.

For details on how to access the raw data that underpins these results please see Appendix A.

Discussion

Techniques that rely on a measurement of R_2' to infer information about deoxyhaemoglobin content are highly dependent on the accurate removal of the effects of macroscopic magnetic field inhomogeneity. Therefore, it is critical to the adoption of these methods that techniques be developed to acquire R_2' weighted data in a simple and robust way. The technique demonstrated in this study combines the benefits of two approaches: (i) through-slice MFGs are prospectively corrected removing the need for post hoc removal of the effect of MFGs or the acquisition of magnetic field maps (i.e. GESEPI (Yang et al., 1998)) and (ii) the R_2' weighted signal is acquired directly with constant R_2 weighting removing the need to simultaneously fit R_2 (i.e. ASE (An and Lin, 2003)). Together these features remove confounding effects from the acquired signal, reducing the need for postprocessing and requiring only a monoexponential fit to produce measurements of R_2'. This could remove one of the barriers to the more widespread adoption of techniques that rely on a measurement of R_2', enabling a broader spectrum of users to take advantage of these methods.

MFG compensation optimisation

Field mapping enabled the range of susceptibility induced MFGs to be quantified. The frontal and temporal lobes were found to have the largest through-slice MFGs, consistent with their location close to the nasal sinuses and ear canals, respectively. The magnitude of these MFGs was summarised using percentiles for a number of cortical ROIs (Table 1). This enabled the GASE sequence to be optimised based on the fraction of uncorrected voxels that may be tolerated in the resulting

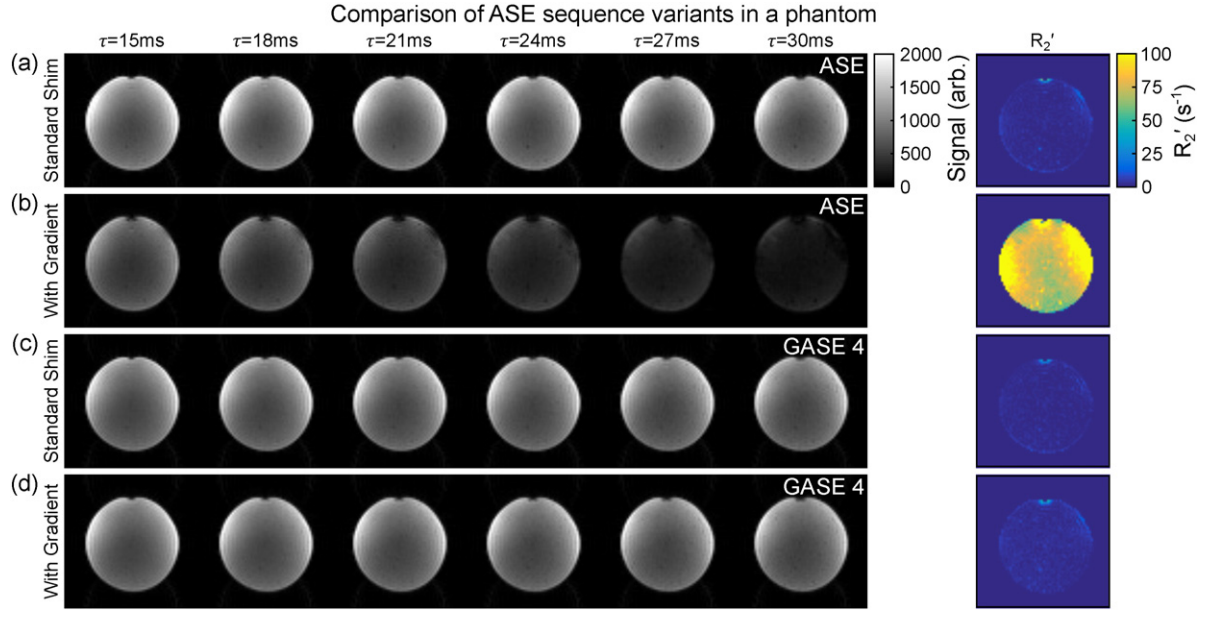

Fig. 2. In order to compare the effectiveness of GESEPI ASE (GASE) with standard ASE, data were acquired from a homogenous phantom. Assuming that the phantom was well shimmed and that contributions to R_2' were minimal, little signal decay should be observed over the range of τ values acquired for either (a) ASE or (c) GASE 4. Imposition of a magnetic field gradient in the z-direction markedly increases signal decay for (b) ASE, but not (d) GASE 4.

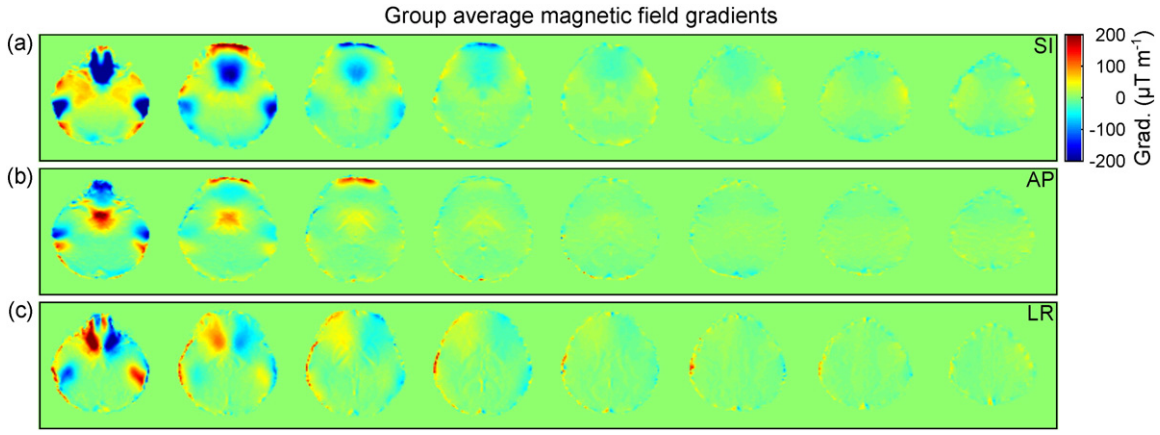

Fig. 3. Maps of the average magnetic field gradient across a group of healthy volunteers in (a) the superior–inferior (SI), (b) anterior–posterior (AP) and (c) left–right (LR) directions.

R_2' maps. Based on this analysis three variants of the GASE sequence were developed; GASE 4, GASE 8 and GASE 128.

Since the critical MFG at the longest τ value for GASE 4 is 313 μT m^{-1}, approximately 95% of the through-slice MFGs observed in the field mapping cohort should be compensated. Whereas the compensation in GASE 8 is twice as high (621 μT m^{-1}) and so should be able to correct for approximately 99% of through-slice MFGs. The GASE 128 variant had the same level of correction in the superior–inferior direction as GASE 4, but increased in-plane resolution in order to increase the tolerance of the method to in-plane MFGs. Again this is equivalent to correcting approximately 95% of in-plane MFGs in GASE 4, whilst GASE 128 should correct for approximately 99%.

Fig. 5 enables us to visualise the regions of the brain that benefit from increasing the level of MFG compensation. Fig. 5a shows regions where R_2' is elevated in the standard ASE pulse sequence compared with GASE 4. These regions are consistent with regions of high through-slice MFGs in Fig. 3a — the group average from the field mapping cohort. Table 2 confirms that all ROIs see a reduction in the median and IQR of R_2' estimates. Similarly, Fig. 5b highlights the regions that benefit from the increased through-slice MFG compensation provided by GASE 8. These areas are small but consistent with the largest MFGs in Fig. 3a. However, Table 2 shows that this results in a minimal reduction in median and IQR of R_2' estimates in any of the ROIs. Finally, Fig. 5c shows the improvement achieved by increasing the in-plane MFG compensation. Areas of reduced R_2' show similarities with the measured in-plane gradients in the group field maps (Fig. 3b, c). The reduction in median and IQR varies by ROI, but is particularly large in the temporal lobes where the highest in-plane MFGs are expected. However, when statistical analysis of the cortex ROI is performed the results of the GASE 8 sequence are not significantly different to GASE 4 ($p = 0.86$). There may be some benefit of the higher in-plane resolution offered by GASE 128, which gave results significantly different to both GASE 4 ($p < 0.0001$) and GASE 8 ($p < 0.0001$).

Table 1
Voxel level analysis of the large scale magnetic field gradients along the three orthogonal axes. Equivalent directions: superior–inferior (SI), — z-axis, anterior–posterior (AP) — y-axis, left–right (LR) — x-axis.

ROI	SI-gradient by percentile (μT m^{-1})						
	0.5	2.5	25	50	75	97.5	99.5
Cerebellum	−291.9	−152.9	−8.4	11.9	42.7	224.6	361.6
Frontal	−512.3	−245.2	−24.3	−1.8	18.3	145.6	328.6
Insula	−55.5	−19.4	3.6	10.9	19.5	60.8	103.1
Occipital	−222.1	−123.0	−15.7	−1.6	11.1	91.9	170.3
Parietal	−112.7	−55.7	−7.2	1.3	11.4	48.8	101.2
Temporal	−438.8	−245.8	−9.3	31.5	85.1	300.9	453.4
Cortex	−425.2	−173.6	−14.4	2.5	22.3	180.1	338.9
ROI	AP-gradient by percentile (μT m^{-1})						
	0.5	2.5	25	50	75	97.5	99.5
Cerebellum	−279.2	−164.5	−44.8	−17.8	−2.4	100.2	211.6
Frontal	−241.5	−129.7	−13.7	−2.1	7.4	107.3	260.4
Insula	−165.6	−42.6	−7.0	−1.1	4.7	31.0	59.8
Occipital	−147.7	−88.6	−17.4	−5.5	4.8	111.2	227.1
Parietal	−76.2	−33.3	−2.4	4.3	11.1	44.1	93.4
Temporal	−394.8	−209.0	−28.0	−1.6	20.3	170.5	351.6
Cortex	−252.6	−122.0	−11.9	−0.3	10.0	107.1	246.4
ROI	LR-gradient by percentile (μT m^{-1})						
	0.5	2.5	25	50	75	97.5	99.5
Cerebellum	−324.4	−163.3	−15.1	0.2	17.0	156.4	298.9
Frontal	−327.0	−125.5	−11.8	2.3	16.3	153.0	350.9
Insula	−77.6	−54.3	−20.1	−5.3	8.0	44.9	64.4
Occipital	−138.8	−82.6	−10.5	−0.6	9.7	90.7	167.0
Parietal	−109.0	−48.6	−7.8	0.1	7.8	69.4	171.7
Temporal	−383.5	−198.9	−30.8	−0.5	31.7	228.2	398.7
Cortex	−287.5	−117.7	−12.6	0.6	13.8	144.4	317.3

This analysis makes it clear that the optimal level of compensation is dependent on the region of the brain that is being investigated. Outside of the frontal and temporal lobes the MFG compensation provided by GASE 4 is likely to be sufficient. However, within these regions higher compensation, and hence longer acquisitions, may be necessary. Unfortunately increasing the level of compensation also penalises regions of the brain that are largely unaffected by MFGs. As the partition thickness is reduced SNR decreases linearly and is only improved as the square root of the number of partitions averaged together. It must also be remembered that if the maximum τ value is increased the level of MFG compensation must also be increased to maintain the same level of correction. Alternatively it may be possible to truncate the acquired data set at the first τ value that exceeds the MFG compensation threshold (Storey et al., 2015).

Comparison with the literature

As detailed in the introduction, multiple techniques have been used to measure R_2'. However, it has been shown that these techniques do not necessarily produce equivalent measurements of R_2' (Ni et al., 2015). Using an ASE pulse sequence, similar to that used in this study, R_2' was measured as 3.04 s^{-1} in a grey matter ROI (An and Lin, 2003). However, it is unclear whether these data were corrected for the effects of magnetic field inhomogeneity and vascular crushers were used to minimise the blood signal contribution. An ASE acquisition generated from multiple GESFIDE acquisitions has been used to measure $R_2' =$ 3.8 s^{-1} in grey matter (Ni et al., 2015). Thin slices were used to minimise the effects of magnetic field inhomogeneity. In the same study measurements were also made using the GESFIDE and GESSE sequences giving values of 2.7 s^{-1} in both cases (Ni et al., 2015). Further GESFIDE

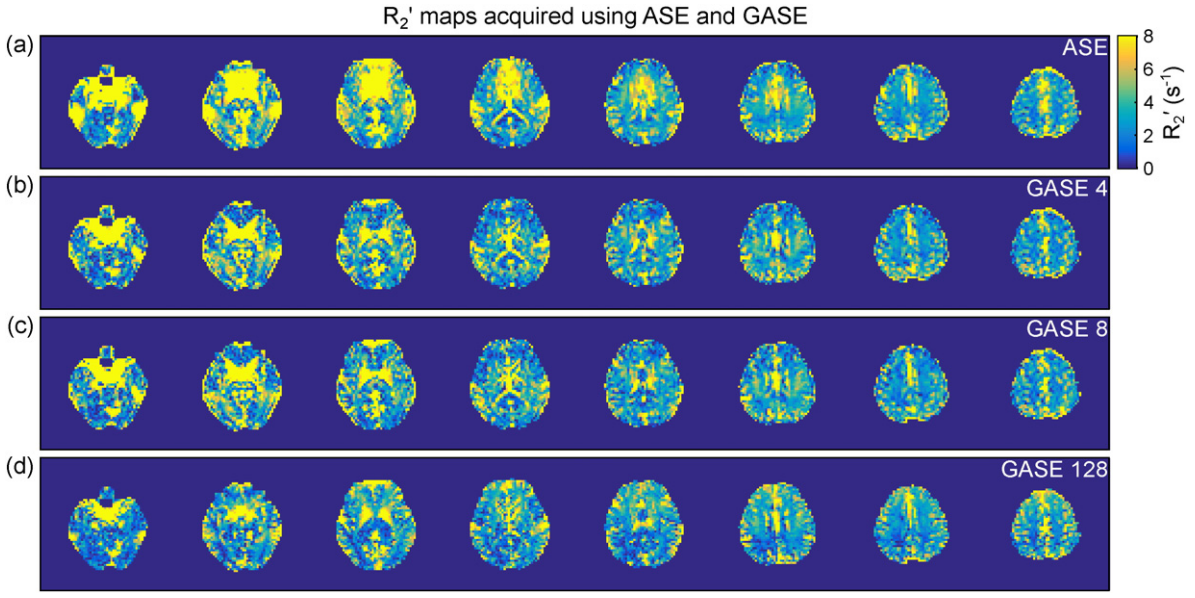

Fig. 4. Maps of R_2' from a single example subject (selected slices spanning the slice coverage in the superior–inferior direction) acquired using (a) standard ASE, (b) GASE 4 (average of four 1.25 mm partitions), (c) GASE 8 (average of eight 0.63 mm slices) and (d) GASE 128 (average of four 1.25 mm partitions and doubled in-plane resolution).

measurements give $R_2' = 3.4\ s^{-1}$ in prefrontal cortex (Gelman et al., 1999) and $R_2' = 2.9\ s^{-1}$ using GESSE in grey matter (He and Yablonskiy, 2007). Thin slices were used to mitigate the effect of field inhomogeneity in the former, whilst correction using an independently acquired field map was performed in the latter. One final category of measurements uses independently acquired maps of R_2 and R_2^* to estimate R_2' by subtraction. Values of 7.1–7.4 s^{-1} in the frontal cortex of 20–30 year olds (Sedlacik et al., 2013) and 9.2 s^{-1} in grey matter (Paling et al., 2012) have been measured. Field map correction was used in the former and high resolution imaging was used to measure R_2^* in the latter. These appreciably higher values of R_2' reveal a broader difficulty in comparing such estimates. In measuring R_2' we typically assume that the signal is monoexponential and that the tissue in the voxel is homogenous. This is clearly not the case as the R_2' weighted signal is known to behave with a quadratic exponential decay at short τ values before transitioning to a linear exponential regime (Yablonskiy and Haacke, 1994). In addition multiple compartments are almost always present containing mixtures of grey matter, white matter, blood and CSF and producing multiexponential decay. These effects are exacerbated in the subtraction technique as the separate R_2 and R_2^* measurements are typically acquired with very different pulse sequence parameters. For example, differences in TR between the measurements alters the weighting of different compartments due to the effect of T_1 and using a different range of echo times in each of the measurements will result in different regions of the multiexponential decay curve being sampled (Fujita et al., 2003). Therefore measurements of R_2' made using the subtraction technique are strongly bound to the parameters of the specific sequences used to acquire maps of R_2 and R_2^*.

In the current study, maps of R_2' were acquired in 2 min 24 s (GASE 4). This is slightly less than previous ASE experiments at 3 min 20 s (An and Lin, 2003), but at the cost of fewer τ values. GESSE/GESFIDE measurements are reported in the range from 4 min 56 s (Ni et al., 2015) to 8 min 30 s (He and Yablonskiy, 2007), whilst measurements using the subtraction technique range from 3 min 13 s (Sedlacik et al., 2013) to 15 min 35 s (Paling et al., 2012). The GASE method is competitive in terms of scan duration, especially when considering that it allows MFGs to be prospectively corrected without the need for a separate field map acquisition.

Table 2
Voxel level analysis of grey matter R_2' values across several regions of interest for different ASE and GASE variants. The "cortex" region of interest contains all regions except the cerebellum.

ROI	R_2' (s^{-1})							
	ASE		GASE 4		GASE 8		GASE 128	
	Median	IQR	Median	IQR	Median	IQR	Median	IQR
Cerebellum	3.62	5.10	2.99	3.81	2.68	3.71	1.98	2.94
Frontal	4.38	5.31	2.96	3.00	3.09	3.19	3.43	3.24
Insula	3.59	2.14	3.24	2.13	2.94	2.41	2.57	2.66
Occipital	3.92	3.98	3.16	3.47	2.95	3.67	2.38	3.33
Parietal	3.81	3.11	3.49	2.88	3.42	3.17	2.88	3.00
Temporal	7.74	17.66	4.76	9.07	4.76	8.89	3.05	4.32
Cortex	4.42	5.70	3.43	3.77	3.42	4.04	2.99	3.44

Limitations and Future work

There are several limitations of the current study. In the initial MFG mapping experiments 2D FLASH based field maps were acquired with a slice thickness of 2 mm. This limits our ability to resolve rapid spatial changes in MFGs. However, we believe that since MFGs are expected to vary smoothly in the vast majority of cases this does not pose a major limitation in this study. Improvements could be made by using a 3D approach and isotropic voxel dimensions.

For the ASE measurements, a relatively small range of τ values were acquired in the range from 15 to 30 ms. The minimum value was chosen to ensure that images were acquired in the linear exponential region of the decay based on the predictions of the static dephasing model (Yablonskiy and Haacke, 1994). However, diffusion around small vessels may mean that this transition occurs at later values of τ (Dickson et al., 2010). The maximum value of τ was dictated by TE, which was chosen to be 44 ms to provide reasonable SNR. Analysis of the GESFIDE sequence suggests that a longer TE could improve SNR further (Song and Song, 2007). Further work is required to perform a similar optimisation for the ASE pulse sequence.

In this work we have concentrated on reducing the effect of MFGs on measurements of R_2'. However, it has also been noted that the presence of CSF partial volumes can confound estimates of R_2' (Dickson et al., 2009; He and Yablonskiy, 2007). In turn this would reduce the specificity of R_2' to deoxyhaemoglobin. This effect could be minimised by the use of a fluid attenuated inversion recovery (FLAIR) preparation (Hajnal et al., 1992). The effect of intravascular signal on the R_2' weighted ASE signal has also been investigated by applying diffusion weighting

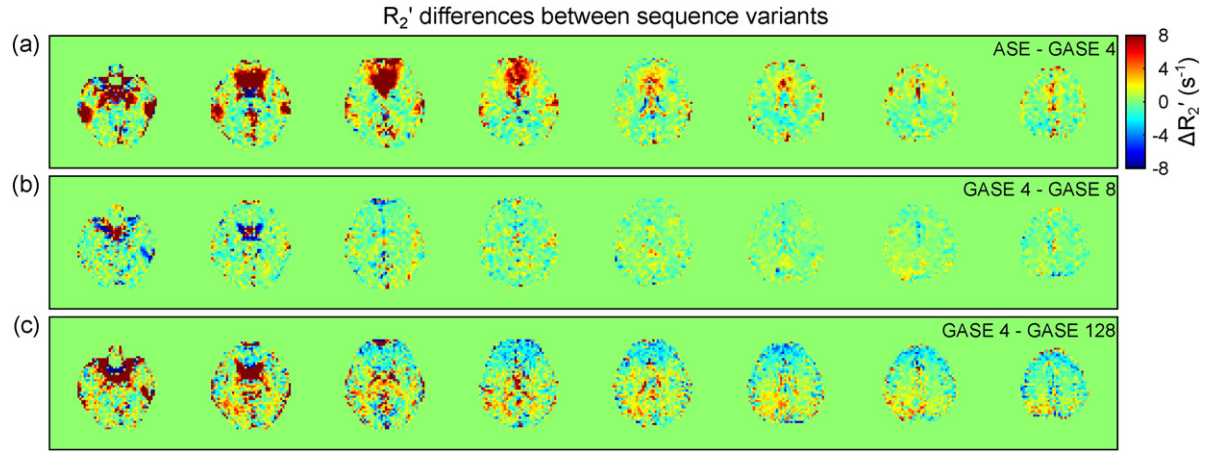

Fig. 5. Regions of the brain that benefit most from prospective magnetic field gradient correction are highlighted by subtracting maps of R_2' made with increasing levels of correction. The largest improvement is made when comparing (a) standard ASE and GASE 4, whilst further improvements are seen in inferior regions of the brain by increasing compensation in (b) the superior–inferior direction (GASE 4–GASE 8) or (c) in-plane dimensions (GASE 4–GASE 128).

to dephase flowing intravascular spins (An and Lin, 2003). Whilst R_2' estimates were not reported, crushing of intravascular signal resulted in reduced estimates of venous cerebral blood volume and increased estimates of OEF as measured by quantitative BOLD.

To reduce Gibb's ringing, a Hanning filter was applied to the raw data during image reconstruction. It has recently been shown that this can result in additional signal attenuation and that a Tukey filter is able to reduce ringing without substantial signal attenuation (Storey et al., 2015).

Conclusions

Prospective correction of macroscopic magnetic field gradients was implemented to improve the specificity of measurements of R_2' to deoxyhaemoglobin content in the brain. This was achieved by combining Gradient-Echo Slice Excitation Profile Imaging (GESEPI) with the Asymmetric Spin Echo (ASE) relaxometry technique. The GESEPI technique provides correction for signal attenuation due to magnetic field gradients below a critical threshold. Below this threshold further correction is not required. When combined with the ASE method, this allows R_2' weighted data to be directly acquired, since the R_2 weighted component is constant, further simplifying the estimation of R_2'. Approaches such as this are the key to increasing the adoption of techniques to measure oxygen metabolism, such as quantitative BOLD (An and Lin, 2000; He and Yablonskiy, 2007) and R_2' based calibrated BOLD (Blockley et al., 2015).

Acknowledgements

This work was funded by EPSRC grant EP/K025716/1.

Appendix A. Supplementary data

The raw data that underpins this work can be accessed via the Oxford Research Archive repository. Doi: http://dx.doi.org/10.5287/bodleian:Py6D0x4EZ.

References

An, H., Lin, W., 2000. Quantitative measurements of cerebral blood oxygen saturation using magnetic resonance imaging. J. Cereb. Blood Flow Metab. 20, 1225–1236. http://dx.doi.org/10.1097/00004647-200008000-00008.

An, H., Lin, W., 2003. Impact of intravascular signal on quantitative measures of cerebral oxygen extraction and blood volume under normo- and hypercapnic conditions using an asymmetric spin echo approach. Magn. Reson. Med. 50, 708–716. http://dx.doi.org/10.1002/mrm.10576.

Blockley, N.P., Griffeth, V.E.M., Buxton, R.B., 2012. A general analysis of calibrated BOLD methodology for measuring $CMRO_2$ responses: comparison of a new approach with existing methods. NeuroImage 60, 279–289. http://dx.doi.org/10.1016/j.neuroimage.2011.11.081.

Blockley, N.P., Griffeth, V.E.M., Simon, A.B., Dubowitz, D.J., Buxton, R.B., 2015. Calibrating the BOLD response without administering gases: comparison of hypercapnia calibration with calibration using an asymmetric spin echo. NeuroImage 104, 423–429. http://dx.doi.org/10.1016/j.neuroimage.2014.09.061.

Collins, D.L., Holmes, C.J., Peters, T.M., 1995. Automatic 3-D model-based neuroanatomical segmentation. Hum. brain.

Constable, R.T., 1995. Functional MR imaging using gradient-echo echo-planar imaging in the presence of large static field inhomogeneities. J. Magn. Reson. Imaging 5, 746–752.

Dickson, J.D., Williams, G.B., Harding, S.G., Carpenter, T.A., Ansorge, R.E., 2009. Nulling the CSF signal in quantitative fMRI. Presented at the Proc. Intl. Soc. Mag. Reson. Med. 17, p. 1640

Dickson, J.D., Ash, T.W.J., Williams, G.B., Harding, S.G., Carpenter, T.A., Menon, D.K., Ansorge, R.E., 2010. Quantitative BOLD: the effect of diffusion. J. Magn. Reson. Imaging 32, 953–961. http://dx.doi.org/10.1002/jmri.22151.

Frahm, J., Merboldt, K.D., Hänicke, W., 1988. Direct FLASH MR imaging of magnetic field inhomogeneities by gradient compensation. Magn. Reson. Med. 6, 474–480.

Friedman, L., Glover, G.H., 2006. Report on a multicenter fMRI quality assurance protocol. J. Magn. Reson. Imaging 23, 827–839. http://dx.doi.org/10.1002/jmri.20583.

Fujita, N., Shinohara, M., Tanaka, H., Yutani, K., Nakamura, H., Murase, K., 2003. Quantitative mapping of cerebral deoxyhemoglobin content using MR imaging. NeuroImage 20, 2071–2083. http://dx.doi.org/10.1016/S1053-8119(03)00399-9.

Gelman, N., Gorell, J.M., Barker, P.B., Savage, R.M., Spickler, E.M., Windham, J.P., Knight, R.A., 1999. MR imaging of human brain at 3.0 T: preliminary report on transverse relaxation rates and relation to estimated iron content. Radiology 210, 759–767. http://dx.doi.org/10.1148/radiology.210.3.r99fe41759.

Hajnal, J.V., Bryant, D.J., Kasuboski, L., Pattany, P.M., De Coene, B., Lewis, P.D., Pennock, J.M., Oatridge, A., Young, I.R., Bydder, G.M., 1992. Use of fluid attenuated inversion recovery (FLAIR) pulse sequences in MRI of the brain. J. Comput. Assist. Tomogr. 16, 841–844.

He, X., Yablonskiy, D.A., 2007. Quantitative BOLD: mapping of human cerebral deoxygenated blood volume and oxygen extraction fraction: default state. Magn. Reson. Med. 57, 115–126. http://dx.doi.org/10.1002/mrm.21108.

Jenkinson, M., Bannister, P., Brady, M., Smith, S., 2002. Improved optimization for the robust and accurate linear registration and motion correction of brain images. NeuroImage 17, 825–841.

Jenkinson, M., Beckmann, C.F., Behrens, T.E.J., Woolrich, M.W., Smith, S.M., 2012. FSL. NeuroImage 62, 782–790. http://dx.doi.org/10.1016/j.neuroimage.2011.09.015.

Ma, J., Wehrli, F.W., 1996. Method for image-based measurement of the reversible and irreversible contribution to the transverse-relaxation rate. J. Magn. Reson. B 111, 61–69.

Mazziotta, J., Toga, A., Evans, A., Fox, P., Lancaster, J., Zilles, K., Woods, R., Paus, T., Simpson, G., Pike, B., Holmes, C., Collins, L., Thompson, P., MacDonald, D., Iacoboni, M., Schormann, T., Amunts, K., Palomero-Gallagher, N., Geyer, S., Parsons, L., Narr, K., Kabani, N., Le Goualher, G., Boomsma, D., Cannon, T., Kawashima, R., Mazoyer, B., 2001. A probabilistic atlas and reference system for the human brain: International Consortium for Brain Mapping (ICBM). Philos. Trans. R. Soc. Lond., B., Biol. Sci. 356, 1293–1322. http://dx.doi.org/10.1098/rstb.2001.0915.

Mugler, J.P., Brookeman, J.R., 1990. Three-dimensional magnetization-prepared rapid gradient-echo imaging (3D MP RAGE). Magn. Reson. Med. 15, 152–157.

Ni, W., Christen, T., Zun, Z., Zaharchuk, G., 2015. Comparison of R2′ measurement methods in the normal brain at 3 Tesla. Magn. Reson. Med. 73, 1228–1236. http://dx.doi.org/10.1002/mrm.25232.

Ordidge, R.J., Gorell, J.M., Deniau, J.C., Knight, R.A., Helpern, J.A., 1994. Assessment of relative brain iron concentrations using T_2-weighted and T_2^*-weighted MRI at 3 Tesla. Magn. Reson. Med. 32, 335–341.

Paling, D., Tozer, D., Wheeler-Kingshott, C., Kapoor, R., Miller, D.H., Golay, X., 2012. Reduced R_2' in multiple sclerosis normal appearing white matter and lesions may reflect decreased myelin and iron content. J. Neurol. Neurosurg. Psychiatry http://dx.doi.org/10.1136/jnnp-2012-302541.

Reichenbach, J.R., Venkatesan, R., Yablonskiy, D.A., Thompson, M.R., Lai, S., Haacke, E.M., 1997. Theory and application of static field inhomogeneity effects in gradient-echo imaging. J. Magn. Reson. Imaging 7, 266–279.

Sedlacik, J., Boelmans, K., Löbel, U., Holst, B., Siemonsen, S., Fiehler, J., 2013. Reversible, irreversible and effective transverse relaxation rates in normal aging brain at 3 T. NeuroImage 1–10 http://dx.doi.org/10.1016/j.neuroimage.2013.08.051.

Smith, S.M., 2002. Fast robust automated brain extraction. Hum. Brain Mapp. 17, 143–155. http://dx.doi.org/10.1002/hbm.10062.

Song, R., Song, H.K., 2007. Echo-spacing optimization for the simultaneous measurement of reversible (R2′) and irreversible (R2) transverse relaxation rates. Magn. Reson. Imaging 25, 63–68. http://dx.doi.org/10.1016/j.mri.2006.09.008.

Storey, P., Lui, Y.W., Novikov, D.S., 2015. Artifact-free T2* mapping without post hoc corrections. Presented at the Proc. Intl. Soc. Mag. Reson. Med., Toronto, p. 442.

Wadghiri, Y.Z., Johnson, G., Turnbull, D.H., 2001. Sensitivity and performance time in MRI dephasing artifact reduction methods. Magn. Reson. Med. 45, 470–476.

Weiskopf, N., Hutton, C., Josephs, O., Turner, R., Deichmann, R., 2007. Optimized EPI for fMRI studies of the orbitofrontal cortex: compensation of susceptibility-induced gradients in the readout direction. Magn. Reson. Mater. Phys. 20, 39–49. http://dx.doi.org/10.1007/s10334-006-0067-6.

Wismer, G.L., Buxton, R.B., Rosen, B.R., Fisel, C.R., Oot, R.F., Brady, T.J., Davis, K.R., 1988. Susceptibility induced MR line broadening: applications to brain iron mapping. J. Comput. Assist. Tomogr. 12, 259–265.

Yablonskiy, D.A., 1998. Quantitation of intrinsic magnetic susceptibility-related effects in a tissue matrix. Phantom study. Magn. Reson. Med. 39, 417–428.

Yablonskiy, D.A., Haacke, E.M., 1994. Theory of NMR signal behavior in magnetically inhomogeneous tissues: the static dephasing regime. Magn. Reson. Med. 32, 749–763.

Yang, Q.X., Williams, G.D., Demeure, R.J., Mosher, T.J., Smith, M.B., 1998. Removal of local field gradient artifacts in T_2^*-weighted images at high fields by gradient-echo slice excitation profile imaging. Magn. Reson. Med. 39, 402–409.

Zhang, Y., Brady, M., Smith, S., 2001. Segmentation of brain MR images through a hidden Markov random field model and the expectation–maximization algorithm. IEEE Trans. Med. Imaging 20, 45–57. http://dx.doi.org/10.1109/42.906424.